

## Competitive Adsorption of HO and CO in 2-Dimensional Nano-Confinement: GCMC Simulations of Cs- and Ca-Hectorite

Narasimhan Loganathan, Geoffrey M Bowers, A. Ozgur Yazaydin, Andrey G. Kalinichev, and R. James Kirkpatrick

*J. Phys. Chem. C*, **Just Accepted Manuscript** • DOI: 10.1021/acs.jpcc.8b06602 • Publication Date (Web): 21 Sep 2018

Downloaded from <http://pubs.acs.org> on September 25, 2018

### Just Accepted

“Just Accepted” manuscripts have been peer-reviewed and accepted for publication. They are posted online prior to technical editing, formatting for publication and author proofing. The American Chemical Society provides “Just Accepted” as a service to the research community to expedite the dissemination of scientific material as soon as possible after acceptance. “Just Accepted” manuscripts appear in full in PDF format accompanied by an HTML abstract. “Just Accepted” manuscripts have been fully peer reviewed, but should not be considered the official version of record. They are citable by the Digital Object Identifier (DOI®). “Just Accepted” is an optional service offered to authors. Therefore, the “Just Accepted” Web site may not include all articles that will be published in the journal. After a manuscript is technically edited and formatted, it will be removed from the “Just Accepted” Web site and published as an ASAP article. Note that technical editing may introduce minor changes to the manuscript text and/or graphics which could affect content, and all legal disclaimers and ethical guidelines that apply to the journal pertain. ACS cannot be held responsible for errors or consequences arising from the use of information contained in these “Just Accepted” manuscripts.



1  
2  
3  
4  
5  
6  
7  
8  
9  
10  
11  
12  
13  
14  
15  
16  
17  
18  
19  
20  
21  
22  
23  
24  
25  
26  
27  
28  
29  
30  
31  
32  
33  
34  
35  
36  
37  
38  
39  
40  
41  
42  
43  
44  
45  
46  
47  
48  
49  
50  
51  
52  
53  
54  
55  
56  
57  
58  
59  
60

# Competitive Adsorption of H<sub>2</sub>O and CO<sub>2</sub> in 2-Dimensional Nano-confinement: GCMD Simulations of Cs- and Ca-Hectorite

*Narasimhan Loganathan<sup>1</sup>, \* Geoffrey M. Bowers<sup>2</sup>, A. Ozgur Yazaydin<sup>1,3</sup>,*

*Andrey G. Kalinichev<sup>4</sup> and R. James Kirkpatrick<sup>1,5</sup>*

<sup>1</sup> Department of Chemistry, Michigan State University, East Lansing, Michigan 48824,  
United States

<sup>2</sup> Department of Chemistry and Biochemistry, St. Mary's College of Maryland, St. Mary's  
City, Maryland 20686, United States

<sup>3</sup> Department of Chemical Engineering, University College London, London, WC1E7JE,  
United Kingdom

<sup>4</sup> Laboratoire SUBATECH (UMR 6457 - Institut Mines-Télécom Atlantique, Université de  
Nantes, CNRS/IN2P3), 44307, Nantes, France

<sup>5</sup> Department of Earth and Environmental Sciences, Michigan State University, East Lansing,  
Michigan 48824, United States

\* **Corresponding author e-mail:** naresh20@msu.edu

**Telephone:** (+1)517-353-1106

**Abstract**

The intercalation of H<sub>2</sub>O, CO<sub>2</sub>, and other fluid species in expandable clay minerals (smectites) may play a significant role in controlling the behavior of these species in geological carbon sequestration and enhanced petroleum production and has been the subject of intensive study in recent years. This paper reports the results of a computational study of the effects of the properties of the charge balancing, exchangeable cations on H<sub>2</sub>O and CO<sub>2</sub> intercalation in the smectite mineral, hectorite, in equilibrium with an H<sub>2</sub>O-saturated supercritical CO<sub>2</sub> fluid under reservoir conditions using Grand Canonical Molecular Dynamics (GCMD) methods. The results show that the intercalation behavior is greatly different for the cations with relatively low hydration energies and high affinities for CO<sub>2</sub> (here Cs<sup>+</sup>) than for cations with higher hydration energies (here Ca<sup>2+</sup>). With Cs<sup>+</sup>, CO<sub>2</sub> intercalation occurs in a 1-layer structure and does not require H<sub>2</sub>O intercalation, whereas with Ca<sup>2+</sup> the presence of a sub-monolayer of H<sub>2</sub>O is required for CO<sub>2</sub> intercalation. The computational results provide detailed structural, dynamical and energetic insight into the differences in intercalation behavior and are in excellent agreement with *in situ* experimental XRD, IR, quartz crystal microbalance, and NMR results for smectite materials obtained under reservoir conditions.

## Introduction

Clay minerals are important components of the deep sedimentary formations that are potential reservoirs for geological CO<sub>2</sub> sequestration and shale/tight gas production.<sup>1-16</sup> The competitive interaction of CO<sub>2</sub> and H<sub>2</sub>O with clays is, thus, central to understanding fluid behavior in these situations. The common smectite and mixed-layer illite-smectite clay minerals contain expandable interlayer galleries that contain intercalated charge balancing cations and variable numbers of fluid molecules. The partitioning of CO<sub>2</sub> and H<sub>2</sub>O between the intergranular pore fluid and the interlayer galleries may be significant in controlling the overall transport and physical properties of the host rock and has been a topic of substantial recent experimental and computational study.<sup>16-42</sup> Due to the presence of two basal surfaces separated by less than one to a few nm, the structure and dynamics of fluids nano-confined in the interlayer galleries are substantially different than on external clay surfaces (interparticle pores) or in the bulk fluid phase. Recent experimental and computational modeling studies have clearly shown that the clay swelling behavior depends strongly on the nature of the charge balancing cation (characterized by the CO<sub>2</sub> and H<sub>2</sub>O solvation energies) and on the composition and location of the permanent structural charge of the clay.<sup>43-57</sup>

Experimental and computational modeling studies have shown that at reservoir conditions the amount of intercalated CO<sub>2</sub> and its structural, dynamical, and energetic properties depend on the basal spacing and the solvation energies of the charge-balancing cation with H<sub>2</sub>O and CO<sub>2</sub> in smectite interlayers under supercritical conditions (scCO<sub>2</sub>,  $T_c \sim 31^\circ\text{C}$ ,  $P_c \sim 73$  bar).<sup>17-42</sup> X-ray diffraction (XRD) studies at pressurized CO<sub>2</sub> conditions by Giesting et al.<sup>18,19</sup> showed that increase (expansion) of the basal spacing of the common smectite, montmorillonite, depends on the initial interlayer H<sub>2</sub>O content. Similar studies by Schaefer et al.<sup>26,28</sup> at 323 K and 90 bar fluid pressure have confirmed that the intercalation of CO<sub>2</sub> in Na-, Ca- and Mg-montmorillonite is possible only when there is at least a sub-

1  
2  
3 monolayer amount of H<sub>2</sub>O that props open the interlayer. For these cations, solvation by H<sub>2</sub>O  
4 is energetically more favorable than by CO<sub>2</sub>. The *in situ* infrared (IR) results of Loring et al.<sup>29-</sup>  
5  
6  
7  
8  
9  
10  
11  
12  
13  
14  
15  
16  
17  
18  
19  
20  
21  
22  
23  
24  
25  
26  
27  
28  
29  
30  
31  
32  
33  
34  
35  
36  
37  
38  
39  
40  
41  
42  
43  
44  
45  
46  
47  
48  
49  
50  
51  
52  
53  
54  
55  
56  
57  
58  
59  
60

monolayer amount of H<sub>2</sub>O that props open the interlayer. For these cations, solvation by H<sub>2</sub>O is energetically more favorable than by CO<sub>2</sub>. The *in situ* infrared (IR) results of Loring et al.<sup>29-</sup><sup>31</sup> for Na-montmorillonite confirmed that a similar minimum content of co-adsorbed H<sub>2</sub>O is necessary to facilitate CO<sub>2</sub> intercalation and demonstrated that at 323 K and 90 bar maximum CO<sub>2</sub> intercalation occurs when the amount of co-adsorbed H<sub>2</sub>O corresponds to a monolayer (1L) hydrate structure. More recently, the *in situ* XRD, IR and nuclear magnetic resonance (NMR) results of Bowers et al.<sup>17</sup> at 323K and 90 bar showed that the solvation properties of the exchangeable cation (Na<sup>+</sup>, Cs<sup>+</sup> or Ca<sup>2+</sup>) significantly affect the structure, dynamics, and energetics of intercalated CO<sub>2</sub> in the similar smectite mineral, hectorite. The results show that interlayers containing large, monovalent cations that have similar solvation energies for H<sub>2</sub>O and CO<sub>2</sub> (such as Cs<sup>+</sup>)<sup>58</sup> intercalate CO<sub>2</sub> even under experimentally dry conditions after vacuum drying. In contrast, with Na<sup>+</sup> and Ca<sup>2+</sup> CO<sub>2</sub> intercalation requires at least a sub-1L of H<sub>2</sub>O to prop open the interlayers. For all these hectorites, the interlayer CO<sub>2</sub> content increases up to the 1L structure and decreases at higher H<sub>2</sub>O contents, as for montmorillonite at the same conditions.<sup>18,26,29</sup> These results emphasize the importance of having molecular scale understanding of the structure, dynamics, and energetics of H<sub>2</sub>O and CO<sub>2</sub> in the interlayers of smectites with exchangeable cations spanning a range of solvation energies with H<sub>2</sub>O and CO<sub>2</sub>.

Computational molecular modeling studies for Na-smectites are in good agreement with the experimental results showing that CO<sub>2</sub> intercalation requires the presence of at least a sub-1WL H<sub>2</sub>O layer.<sup>33-37,40</sup> Grand Canonical Monte Carlo (GCMC) simulations by Botan et al.<sup>33</sup> also suggest a stable bilayer (2L) hydrate structure (basal spacing ~15.0Å) for Na-montmorillonite at 348 K and 125 bar in contact with H<sub>2</sub>O-saturated scCO<sub>2</sub>. The GCMC simulations of Rao et al.<sup>37</sup> reported a higher interlayer CO<sub>2</sub> mole fraction for Na-montmorillonite with lower structural charge than with higher ones (-0.75 |e| vs. -1.0 |e|) at a given relative humidity (R.H.) at 323 K and 90 bar. Gibbs Ensemble Monte Carlo studies of

1  
2  
3 Makaremi et al.<sup>36</sup> showed how the location of the structural charge sites in the smectite  
4 framework T-O-T layer structure alters the equilibrium basal spacing and energetics of Na-  
5 smectites at 348 K and 125 bar. Our previous grand canonical molecular dynamics (GCMD)  
6 simulations showed that temperature (323-368 K) and pressure (90-150 bar) have little impact  
7 on the structure and dynamics of interlayer CO<sub>2</sub> in Na-hectorite in contact with H<sub>2</sub>O saturated  
8 scCO<sub>2</sub>.<sup>40</sup>  
9

10  
11  
12  
13  
14  
15  
16  
17 There are, however, few computational modeling studies that examine the effect of  
18 cation solvation energy on the partitioning of H<sub>2</sub>O and CO<sub>2</sub> between smectite interlayers and  
19 bulk fluid and its interlayer structure, dynamics, and energetics in the supercritical regime. To  
20 our knowledge, the only such study is that of Kadoura et al.,<sup>34</sup> who explored the influence of  
21 Na<sup>+</sup>, Ca<sup>2+</sup> and Mg<sup>2+</sup> on CO<sub>2</sub> intercalation in montmorillonite at 323 K and 90 bar using GCMC.  
22 The results show that the interlayer CO<sub>2</sub> mole fraction is very similar with all these cations at  
23 R.H.s  $\geq$  60%, consistent with their high affinity for H<sub>2</sub>O. In contrast, our recent *in situ* XRD,  
24 IR and NMR experiments and GCMD simulations with montmorillonite and hectorite have  
25 shown that cations with low hydration energies (e.g., Cs<sup>+</sup>, K<sup>+</sup>, NH<sub>4</sub><sup>+</sup>) permit CO<sub>2</sub> intercalation  
26 even in the absence of H<sub>2</sub>O at 323 K and 90 bar in smectites, whereas those cations with higher  
27 hydration energies (e.g., Na<sup>+</sup>, Ca<sup>2+</sup>, Mg<sup>2+</sup>) do not.<sup>41,42</sup> Energetically, the results show that the  
28 clay-cation interactions play a dominant role in determining the overall intercalation behavior,  
29 suggesting that further studies should be performed for cations with a greater range of size,  
30 CO<sub>2</sub> and H<sub>2</sub>O solvation energies.<sup>41,42</sup>  
31  
32  
33  
34  
35  
36  
37  
38  
39  
40  
41  
42  
43  
44  
45  
46  
47  
48

49 We address this gap here by examining the intercalation behavior of H<sub>2</sub>O and CO<sub>2</sub> in  
50 hectorite containing a cation with a low hydration energy (Cs<sup>+</sup>) and one with a high hydration  
51 energy (Ca<sup>2+</sup>) at 323 K and 90 bar in equilibrium with H<sub>2</sub>O-saturated scCO<sub>2</sub> using GCMD  
52 simulations.<sup>40-42</sup> Cs<sup>+</sup> and Ca<sup>2+</sup> are representative of cations with greatly different hydration  
53 energies and charge/radius ratios,<sup>48,53,58</sup> and they have greatly different CO<sub>2</sub>/H<sub>2</sub>O intercalation  
54  
55  
56  
57  
58  
59  
60

1  
2  
3 behavior.<sup>17</sup> The results here are in excellent agreement with experimental data of Bowers et  
4 al.<sup>17</sup> and provide a basis for their detailed molecular scale structural, dynamic, and energetic  
5 interpretation and understanding.  
6  
7  
8

9  
10 The primary reason for using hectorite rather than montmorillonite is that samples of  
11 natural hectorite with a very low Fe content are available, and such samples were used in NMR  
12 experiments to reduce paramagnetic effects on the probe nuclei.<sup>17</sup> Both hectorite and  
13 montmorillonite develop their layer charge dominantly in the octahedral layer, and previous  
14 experimental NMR, IR, XRD, neutron scattering and simulation studies have shown that their  
15 intercalation behavior is very similar when fully hydroxylated and possessing identical layer  
16 charge.<sup>17-23, 25-54</sup>  
17  
18  
19  
20  
21  
22  
23  
24  
25

## 26 **Simulation Details**

27  
28 Hectorite is a 2:1 trioctahedral smectite that develops its negative structural layer charge  
29 by isomorphic substitution of  $\text{Li}^+$  for  $\text{Mg}^{2+}$  in the octahedral layer. The simulated hectorite  
30 model has a structural formula of  $\text{M}^+(\text{Mg}_5\text{Li})\text{Si}_8\text{O}_{20}(\text{OH})_4$ . There are no tetrahedral  
31 substitutions in this model, in accordance with the experimental sample that contains a  
32 negligible fraction (0.25%) of isomorphic  $\text{Al}^{3+}/\text{Si}^{4+}$  substitution.<sup>59</sup> However, there are two  
33 important differences between the natural sample used in our experiments and the simulated  
34 model: (i) the model has 30% higher layer charge, and (ii) the simulated octahedral layer has  
35 only  $\text{OH}^-$  groups, whereas the natural sample has  $\sim 55\%$   $\text{F}^-$  for  $\text{OH}^-$  substitution.<sup>17,46,47</sup> The  
36 hydration behavior of synthetic fluoro-hectorite has been discussed previously.<sup>60</sup>  
37  
38  
39  
40  
41  
42  
43  
44  
45  
46  
47  
48

49 The simulation supercells for the Cs- and Ca-hectorite models consist of 16  
50 crystallographic unit cells of hectorite ( $4 \times 2 \times 2$ ) and include two interlayer galleries with  
51 surface areas of  $\sim 20.9 \text{ \AA} \times 18.2 \text{ \AA}$  ( $a=b=c: 90^\circ$ ) that are large enough to overcome any finite  
52 size effects. The isomorphic  $\text{Li}^+$  for  $\text{Mg}^{2+}$  substitutions were introduced only after constructing  
53 the supercell. This procedure provides a quasi-disordered pattern with different arrangements  
54  
55  
56  
57  
58  
59  
60

1  
2  
3 of  $\text{Li}^+$  ions in the octahedral layer. Li-O-Li linkages are forbidden in this procedure in  
4  
5 accordance with the generalization of Lowenstein's rule.<sup>61</sup> The initial structure has the charge  
6  
7 compensating cations placed randomly in the interlayer region. Further details about this  
8  
9 hectorite model are described elsewhere.<sup>40,42,49,51</sup>

12 We performed the GCMD<sup>62</sup> simulations in the grand canonical ensemble at 323 K and  
13  
14 90 bar using methods described previously.<sup>40,42</sup> Briefly, the interlayer basal spacings were  
15  
16 varied from 9.2 Å to 18.0 Å at an interval of 0.2 Å. The interlayer galleries were constrained  
17  
18 to maintain the same interlayer spacing along the  $z$ -dimension in each simulation run. However,  
19  
20 the simulations allow the lateral movement of the T-O-T layers along the  $x$  and  $y$  directions  
21  
22 without disrupting the structure or changing the basal spacing. This is because the minimum  
23  
24 energy interlayer structure depends strongly on the relative positions of adjacent T-O-T layers  
25  
26 and varies with the nature of the interlayer cation and the number of intercalated fluid  
27  
28 molecules.<sup>33,40</sup> All the simulations were performed using the GCMD module embedded in the  
29  
30 simulation package, RASPA.<sup>63</sup> The interatomic interactions for the clay structure and the  
31  
32 exchangeable cations are calculated using the *CLAYFF* force field,<sup>64</sup> which is widely used in  
33  
34 clay interfacial simulations. The  $\text{H}_2\text{O}$  and  $\text{CO}_2$  molecules were represented by the rigid versions  
35  
36 of the SPC<sup>65</sup> and EPM2<sup>66</sup> models, respectively. Three-dimensional periodic boundary  
37  
38 conditions were employed with a cutoff of 9.0 Å for short range non-electrostatic interactions,  
39  
40 and the long-range electrostatic interactions were computed using Ewald summation<sup>67</sup> with an  
41  
42 accuracy of  $10^{-6}$ .  
43  
44  
45  
46  
47  
48

49 The composition of the virtual reservoir representing the bulk  $\text{H}_2\text{O}$ - $\text{CO}_2$  fluids  
50  
51 corresponds to the  $\text{H}_2\text{O}$ -saturated  $\text{CO}_2$ -rich phase at the simulated pressure (90 bar) and  
52  
53 temperature (323 K). The values were obtained from the experimental solubility data of  
54  
55 Spycher et al.<sup>68</sup> ( $x_{\text{H}_2\text{O}} = 0.0041$   $x_{\text{CO}_2} = 0.9959$ ). Fugacities required to calculate the probability  
56  
57 of acceptance and deletion moves of the fluid species ( $f_{\text{H}_2\text{O}} = 0.231$ :  $f_{\text{CO}_2} = 0.654$ ) were obtained  
58  
59  
60



1  
2  
3 using the Peng-Robinson equation of state.<sup>69</sup> Further details of the GCMC approach and data  
4 analysis have been discussed in our previous papers.<sup>40,42,49,51,70,71</sup>  
5  
6

## 7 **Results and Discussion**

### 8 *Adsorption Profiles and Energetics*

9  
10 The computed intercalation behavior of CO<sub>2</sub> and H<sub>2</sub>O are very different in the Cs- and  
11 Ca-hectorites (Figures 1a -1c). For both systems, neither H<sub>2</sub>O nor CO<sub>2</sub> intercalate at basal  
12 spacings less than 10.2 Å, but their behaviors are very different as the interlayers expand  
13 (Figures 1a and 1b). For Ca-hectorite, H<sub>2</sub>O adsorption begins at 10.2 Å and reaches a plateau  
14 at ~11.0 Å, where CO<sub>2</sub> intercalation begins (Figure 1a). With increasing basal spacing, the  
15 amount of intercalated CO<sub>2</sub> increases, reaches a maximum at 12.8 Å, gradually decreases at  
16 larger spacings, and finally reaches an approximately constant value of 0.2 CO<sub>2</sub>/unit cell at  
17 spacings > ~16.0 Å. In contrast, the amount of intercalated H<sub>2</sub>O remains almost constant at  
18 spacings between 11.0 Å and 12.8 Å, and then increases almost linearly with further increase  
19 of the interlayer spacing. Based on our previous studies of hydrated Ca-hectorite without CO<sub>2</sub>,<sup>51</sup>  
20 the amount of H<sub>2</sub>O (~3 molecules/unit cell) in the plateau region corresponds to approximately  
21 1/3 of that needed for a full monolayer hydrate structure. This result is in good agreement with  
22 experimental studies that show CO<sub>2</sub> intercalation in Ca-hectorite begins only with H<sub>2</sub>O present  
23 in the interlayer.<sup>17</sup> The decrease in interlayer CO<sub>2</sub> mole fraction with increasing H<sub>2</sub>O content  
24 is consistent with previous IR spectroscopic data for hectorite and similar smectites  
25 (montmorillonite).<sup>17,29-31</sup> The experimentally determined Ca-hectorite basal spacings of  
26 ~12.6 Å and ~15.9 Å correspond to 1L and 2L structures, respectively, and are in very good  
27 agreement with the simulated values of 12.8 Å and 16.2 Å.<sup>17</sup> These 1L and 2L distances are  
28 also comparable to those from our recent MD simulations of hydrated Ca-hectorite without  
29 CO<sub>2</sub> at ambient conditions.<sup>51</sup> Importantly, the adsorption profiles of CO<sub>2</sub> and H<sub>2</sub>O reported here  
30 are similar to our previous studies on Na-hectorite under identical thermodynamic conditions.  
31  
32  
33  
34  
35  
36  
37  
38  
39  
40  
41  
42  
43  
44  
45  
46  
47  
48  
49  
50  
51  
52  
53  
54  
55  
56  
57  
58  
59  
60

1  
2  
3 This similarity emphasizes the critical role played by the H<sub>2</sub>O molecules in propping open the  
4 interlayer region to allow CO<sub>2</sub> intercalation when the interlayer cations have relatively high  
5 hydration energies.<sup>40,58</sup>  
6  
7  
8  
9

10 In contrast, for Cs-hectorite neither H<sub>2</sub>O nor CO<sub>2</sub> intercalate at basal spacings <11.1 Å.  
11 With increasing basal spacing beyond this value, CO<sub>2</sub> intercalation increases up to 12.5 Å,  
12 decreases at larger values, has a shallow local minimum near 14.2 Å, and reaches a nearly  
13 constant value of ~0.3 CO<sub>2</sub>/unit cell at spacings > 16.0 Å (Figure 1b). Significant H<sub>2</sub>O  
14 intercalation begins only at ~13.0 Å, near the maximum of CO<sub>2</sub> intercalation, and increases  
15 with increasing basal spacing. The amount of intercalated H<sub>2</sub>O at spacings < 13.0 Å is  
16 negligible (1.5%), consistent with the experimentally observed intercalation of CO<sub>2</sub> in Cs-  
17 hectorite under fully dry conditions with a basal spacing of 12.2 Å, indicative of an anhydrous  
18 1L structure.<sup>17</sup> At basal spacings > 13.2 Å, the decrease in CO<sub>2</sub> intercalation is compensated  
19 by increasing H<sub>2</sub>O. The adsorption profiles and the interlayer distance at which CO<sub>2</sub>  
20 intercalation begins reported here are very similar those in our earlier study of Cs-hectorite  
21 exposed to dry scCO<sub>2</sub><sup>42</sup> up to 13.2 Å, suggesting that the intercalation behavior of CO<sub>2</sub> is not  
22 significantly affected by the presence of H<sub>2</sub>O in the bulk fluid phase reservoir. Similar increases  
23 in interlayer H<sub>2</sub>O content at larger spacings have been reported previously in simulations of  
24 hydrated Cs-hectorite and other smectites,<sup>49,54</sup> although such expanded structures are not  
25 observed experimentally.  
26  
27  
28  
29  
30  
31  
32  
33  
34  
35  
36  
37  
38  
39  
40  
41  
42  
43  
44  
45  
46

47 The calculated immersion energies for Cs-hectorite (Figure 1c) show a global minimum  
48 at a basal spacing of ~12.5 Å, indicating that the 1L structure is the thermodynamically stable  
49 state for this phase in equilibrium with H<sub>2</sub>O-saturated scCO<sub>2</sub> at 323 K and 90 bar, in agreement  
50 with the experimental results.<sup>17</sup> In contrast, for Ca-hectorite the energy minimum near the 1L  
51 structure is poorly localized. The immersion energies decrease beyond the 1L structure and  
52 reach a minimum at 16.2 Å, corresponding to a 2L structure. Further increase in basal spacing  
53  
54  
55  
56  
57  
58  
59  
60

1  
2  
3 shows little variation in energy, consistent with experimental observations that higher  
4 hydration states for Ca-hectorite are possible, depending upon the thermodynamic activity of  
5 H<sub>2</sub>O.<sup>17</sup> Most importantly, these results clearly demonstrate that the thermodynamically stable  
6 state of Ca-hectorite in equilibrium with H<sub>2</sub>O-saturated scCO<sub>2</sub> has a much larger basal spacing  
7 than Cs-hectorite under the same conditions, consistent with experimental XRD  
8 measurements.<sup>17</sup> The qualitative behavior of the immersion energies of Ca-hectorite are also  
9 consistent with our previous MD simulations of hydrated Ca-hectorite without CO<sub>2</sub>.<sup>51</sup> Ideally,  
10 formation of the stable energy structures can be obtained by computing the disjoining pressure  
11 and swelling free energy calculations.<sup>72,73</sup> However, the results of Young et al.<sup>71</sup> for hydrated  
12 smectites indicate that conclusions drawn from the immersion energies and free energies are  
13 comparable to each other. The use of immersion energies to investigate the equilibrium states  
14 of smectites have been discussed elsewhere for H<sub>2</sub>O adsorption and is extended to CO<sub>2</sub> in our  
15 studies.<sup>49,51,70</sup> Importantly, the thermodynamic stable states obtained using the immersion  
16 energy criterion in our earlier studies of Na-hectorite under identical simulated conditions are  
17 comparable with the conclusions based on swelling free energies reported using the similar  
18 smectite mineral, montmorillonite.<sup>33,36,37,40,42</sup> Therefore, we conclude that the energetic features  
19 of the immersion energy plots are good indicators of the thermodynamically stable states.  
20  
21  
22  
23  
24  
25  
26  
27  
28  
29  
30  
31  
32  
33  
34  
35  
36  
37  
38  
39  
40

41  
42 The computed interlayer CO<sub>2</sub> mole fractions in Cs- and Ca-hectorite are in good  
43 agreement with the ranges estimated from *in situ* high *T* and *P* experimental studies conducted  
44 at similar *T* and *P* conditions<sup>17</sup> (Table 1). For Cs-hectorite, our simulations indicate a CO<sub>2</sub> mole  
45 fraction of 0.98 at the equilibrium 1L basal spacing of 12.5 Å, in reasonable agreement with  
46 the upper-range experimental value of 0.82 estimated from the intensities of the spinning side  
47 bands (SSBs) in <sup>13</sup>C NMR spectra and the IR observed H<sub>2</sub>O/cation ratio.<sup>17</sup> Similarly, for Ca-  
48 hectorite the computed CO<sub>2</sub> mole fractions of 0.34 for the 1L (12.8 Å) structure and 0.02 for  
49 the 2L (16.2 Å) structure are within the ranges estimated from NMR/IR data, though we note  
50  
51  
52  
53  
54  
55  
56  
57  
58  
59  
60

1  
2  
3 that the 2L result is close to what was reported as the minimum interlayer mole fraction for this  
4 sample.<sup>17</sup> The differences between the experimental and computed results for both Cs- and Ca-  
5 hectorite are mostly likely associated with uncertainty in the IR-derived H<sub>2</sub>O/cation ratio due  
6 difficulty in resolving signal from CO<sub>2</sub> sorbed on external surfaces and in interlayers, the layer  
7 charge differences between SHCa-1 and the model (-0.75 |e| vs -1.0 |e|), and the use of a fully  
8 hydroxylated hectorite model in contrast to the extensively fluorinated experimental sample.<sup>17</sup>  
9 Because of the higher structural charge used in the simulations, the model requires more Ca<sup>2+</sup>  
10 ions to charge compensate the surface. Due to the high hydration energy of Ca<sup>2+</sup>,<sup>58</sup> more H<sub>2</sub>O  
11 molecules are adsorbed in the interlayer region to hydrate these Ca<sup>2+</sup> ions leading to less  
12 available space for CO<sub>2</sub> intercalation in the simulation. The effect of charge was been reported  
13 previously by Rao et al.<sup>37</sup> for a similar smectite mineral, montmorillonite. In addition, the XRD  
14 profiles of Dazas et al.<sup>74</sup> clearly indicate that adsorption of H<sub>2</sub>O is less for fluorinated hectorite  
15 compared to hydroxylated hectorite. As a result, there is probably more interlayer space  
16 available for CO<sub>2</sub> intercalation in the experimental sample than in our simulated model.<sup>17</sup>  
17 Because the natural samples inevitably adsorb fluid species on external surfaces, the  
18 simulations provide specific insight into the interlayer fluid composition and dynamics.

19  
20  
21  
22  
23  
24  
25  
26  
27  
28  
29  
30  
31  
32  
33  
34  
35  
36  
37  
38  
39  
40 Importantly, for the 1L structures, which for each cation have the greatest interlayer  
41 CO<sub>2</sub> contents, both Cs- and Ca-hectorite have more interlayer CO<sub>2</sub> than Na-hectorite, as also  
42 observed in the experimental high *T* and *P* IR results.<sup>17,40</sup> Recent GCMC simulation studies by  
43 Kadoura et al.<sup>34</sup> show similar behavior, with Ca- and Mg-montmorillonite having higher CO<sub>2</sub>  
44 mole fractions than Na- montmorillonite at a given R.H. The interlayer CO<sub>2</sub> mole fractions  
45 from our studies for Ca-hectorite are similar to the reported values by Kadoura et al.<sup>34</sup> for Ca-  
46 montmorillonite, despite our simulations having a higher layer charge.

### 47 *Interlayer Structure*

48  
49  
50  
51  
52  
53  
54  
55  
56  
57  
58  
59  
60

1  
2  
3 As for the adsorption isotherms, the atomic density profiles (ADPs) of the intercalated  
4 species as functions of distance normal to the basal surface are greatly different for Cs- and  
5 Ca-hectorite (Figures 2a-2c). For the 1L structures, the presence of H<sub>2</sub>O in Ca-hectorite leads  
6 to a more complex interlayer structure than for Cs-hectorite, which has only ~1.5% interlayer  
7 H<sub>2</sub>O and, thus, does not yield an observable H<sub>2</sub>O ADP. For both 1L phases, the ADPs of the  
8 cation (Ca<sup>2+</sup> or Cs<sup>+</sup>), C<sub>CO2</sub> and O<sub>CO2</sub> are characterized by single peaks located at the mid-plane  
9 of the interlayer (Figures 2a and 2c) coordinating directly with the basal surface. This  
10 arrangement is the same as in Cs-hectorite exposed to dry scCO<sub>2</sub> at the same T and P.<sup>42</sup> For the  
11 1L structure of Ca-hectorite, the nearest neighbor Ca<sup>2+</sup> coordination shell (Figure 3d) consists  
12 of 6.0 H<sub>2</sub>O (3 associated with each surface) and 2.0 O<sub>b</sub> (one from each surface), and the ADPs  
13 of O<sub>H2O</sub> and H<sub>H2O</sub> are characterized by 4 and 5 peaks respectively. As shown in our previous  
14 simulations of hydrated Ca-hectorite without CO<sub>2</sub>,<sup>51</sup> these distributions indicate two different  
15 adsorption environments for H<sub>2</sub>O, one close to the basal surface and the other near the mid-  
16 plane of the interlayer. The H<sub>2</sub>O molecules closer to the surface are coordinated to the oxygen  
17 atoms of the basal surface, O<sub>b</sub>, through both of their H<sub>H2O</sub>. Those near the mid-plane are  
18 coordinated to the O<sub>b</sub> atoms through only one H<sub>H2O</sub> at a time. The H<sub>2</sub>O APDs have been  
19 discussed in more detail in our earlier study.<sup>51</sup> Although the 2L structure is the  
20 thermodynamically stable state for Ca-hectorite in contact with H<sub>2</sub>O-saturated scCO<sub>2</sub> at our  
21 conditions, the structure and dynamics for the 1L state are relevant, because experimental XRD  
22 studies show that it occurs in the presence of H<sub>2</sub>O-undersaturated scCO<sub>2</sub> (low R.H.  
23 conditions).<sup>17</sup> We use the basal spacing of 12.8 Å to represent the 1L structure because it has  
24 the maximum amount of interlayer CO<sub>2</sub> and a complete 1L structure. This 1L structure is  
25 comparable to the experimental structure of Ca-hectorite upon exposure to dry scCO<sub>2</sub> (0 %  
26 R.H.), in which the interlayer spacing corresponds to 1L regime and has a maximum CO<sub>2</sub>  
27 content.<sup>17</sup>  
28  
29  
30  
31  
32  
33  
34  
35  
36  
37  
38  
39  
40  
41  
42  
43  
44  
45  
46  
47  
48  
49  
50  
51  
52  
53  
54  
55  
56  
57  
58  
59  
60

1  
2  
3 In the 2L structure of Ca-hectorite (Figure 2b),  $\text{Ca}^{2+}$  occurs at the mid-plane of the  
4 interlayer  $\sim 4.8$  Å from the two basal surfaces and is coordinated by 8.0  $\text{H}_2\text{O}$  (4 associated with  
5 each basal surface) in a square antiprism arrangement (Figure 3f), consistent with recent high  
6  $T$ - $P$  NMR studies.<sup>17</sup> In contrast, the  $\text{C}_{\text{CO}_2}$  and  $\text{O}_{\text{CO}_2}$  ADP peaks at 3.0 Å and 6.7 Å show that  
7 the  $\text{CO}_2$  molecules are in direct coordination with the basal surfaces. In addition, the broad  
8 shoulders for  $\text{O}_{\text{CO}_2}$  at  $\sim 2.2$  Å and  $\sim 7.5$  Å, even closer to the nearest basal surface, shows that  
9 the  $\text{CO}_2$  molecules probe more orientations and are less dynamically restricted in the 2L  
10 structure than in the 1L structure. As in the 1L structure, the  $\text{H}_2\text{O}$  molecules at 2.8 Å from each  
11 basal surface are coordinated to the  $\text{O}_b$  atoms through one H-atom. In contrast,  $\text{H}_2\text{O}$  molecules  
12 in the mid-plane region (at  $\sim 5.0$  Å) are coordinated only to other  $\text{H}_2\text{O}$  molecules and the  $\text{Ca}^{2+}$ ,  
13 and not to the basal surfaces. The  $\text{Ca}^{2+}$  and  $\text{CO}_2$  distributions are in reasonable agreement with  
14 previous simulations of Ca-montmorillonite in contact with  $\text{scCO}_2$  under similar conditions.<sup>34</sup>  
15 However, our hectorite simulations show only one ADP peak for  $\text{Ca}^{2+}$  in the 1L and 2L  
16 structures, and consequently different  $\text{H}_2\text{O}$  profiles. This difference is probably due to the  
17 presence of tetrahedral charge resulting from Al for Si substitution in the montmorillonite  
18 model used by Kadoura et al.<sup>34</sup> and to the smaller layer charge ( $-0.8 |e|$ ) compared to our model  
19 ( $-1.0 |e|$ ). The presence of tetrahedral charge can greatly change the interlayer adsorption,  
20 structure, and dynamics of  $\text{CO}_2$  and  $\text{H}_2\text{O}$  molecules, as discussed by Makaremi et al.<sup>36</sup> It should  
21 be noted that the interlayer arrangements of  $\text{CO}_2$  molecules in Ca-hectorite in both the 1L and  
22 2L structures are similar to the comparable systems with  $\text{Na}^+$ , although the  $\text{H}_2\text{O}$  distributions  
23 are different because the larger  $\text{H}_2\text{O}$  content in the present study leads to a more ordered  
24 interlayer  $\text{H}_2\text{O}$  structure than in Na-hectorite.<sup>40</sup>

25  
26  
27  
28  
29  
30  
31  
32  
33  
34  
35  
36  
37  
38  
39  
40  
41  
42  
43  
44  
45  
46  
47  
48  
49  
50  
51  
52  
53  
54 In the 1L structure of Cs-hectorite and the 1L and 2L structures of Ca-hectorite, the  
55 computations show that intercalated  $\text{CO}_2$  molecules are oriented with the average position of  
56 their O-C-O vectors parallel to the basal surface (Figure 2d) and that they undergo librational  
57  
58  
59  
60

1  
2  
3 motion around an axis perpendicular to their O-C-O axis. The values 0 and  $\pm 1$  for  $P(\cos \vartheta)_{\text{CO}_2}$   
4  
5 correspond to parallel and perpendicular orientation of  $\text{CO}_2$  with respect to the plane of the  
6  
7 basal surface, respectively. These results are in full agreement with the interpretation of  
8  
9 spinning sideband patterns in *in situ* experimental  $^{13}\text{C}$  MAS NMR spectra.<sup>17</sup> In addition, the  
10  
11 calculations show that the O-C-O axes probe a range of angles, demonstrating wobbling  
12  
13 motion with respect to the basal surfaces. For Ca-hectorite, the angular distribution is larger for  
14  
15 the 2L structure (between  $\sim\pm 0.8$ ) than for the 1L structure (between  $\sim\pm 0.6$ ). The range of  
16  
17 orientations probed by the O-C-O vectors in the 1L structure of Cs-hectorite is essentially  
18  
19 identical to that of the same hectorite model exposed to dry  $\text{scCO}_2$  under similar conditions.<sup>42</sup>  
20  
21 This is as expected due to the very low  $\text{H}_2\text{O}$  content of the structure here. In contrast, the range  
22  
23 of angles explored by the O-C-O vector in the 1L structure of Ca-hectorite is larger than in the  
24  
25 1L structure of the same model exposed to dry  $\text{scCO}_2$  at the same  $P$  and  $T$ .<sup>42</sup> This difference is  
26  
27 most likely due to the combination of a slightly larger basal spacing ( $0.4\text{\AA}$ ) and a higher  
28  
29 interlayer  $\text{CO}_2$  mole fraction (1.0) with dry  $\text{scCO}_2$  compared to our 1L simulations here (0.34)  
30  
31 caused by the presence of interlayer  $\text{H}_2\text{O}$ . In the current study, the  $\text{Ca}^{2+}$  ions are coordinated  
32  
33 by only  $\text{H}_2\text{O}$  molecules and basal oxygen atoms, which permits the intercalated  $\text{CO}_2$  molecules  
34  
35 to occupy the volume between hydrated metal cations. As also found in molecular simulations  
36  
37 of Na-hectorite,<sup>40</sup> the intercalated  $\text{CO}_2$  molecules in the Cs- and Ca-hectorite simulations do  
38  
39 not undergo isotropic reorientation, as shown by the lack of peaks or shoulders near -1 and +1  
40  
41 for the O-C-O vectors. The average angles probed by the  $\text{H}_2\text{O}$  dipole vectors for the 1L and 2L  
42  
43 structures of Ca-hectorite are similar to those in Na-hectorite, demonstrating two different  $\text{H}_2\text{O}$   
44  
45 orientations, consistent with the presence of two different types of interlayer  $\text{H}_2\text{O}$  (Figure S1  
46  
47 and related discussion in the Supporting Information).<sup>40</sup>  
48  
49  
50  
51  
52  
53  
54  
55

56 The radial distribution functions (RDFs) and running coordination numbers (RCNs;  
57  
58 Figures 3a, 3c, 3e) clearly show that the intercalated  $\text{CO}_2$  directly coordinates  $\text{Cs}^+$  in the 1L  
59  
60

1  
2  
3 Cs-hectorite structure (Figure 3b) and that it does not coordinate  $\text{Ca}^{2+}$  in either the 1L or 2L  
4 structures, even for short times (Figures 3d and 3f). For the Cs-hectorite 1L structure, the mean  
5  
6  $\text{Cs}^+ - \text{O}_{\text{CO}_2}$  and  $\text{Cs}^+ - \text{O}_b$ , interatomic distances are both  $\sim 3.2 \text{ \AA}$ . The  $\text{Cs}^+ - \text{O}_b$  RCN is 8.3, and  
7  
8 the  $\text{Cs}^+ - \text{O}_{\text{CO}_2}$  RCN is 4.5, resulting in a total ion coordination number of  $\sim 12.8$ . Each  $\text{Cs}^+$  ion  
9  
10 is in inner sphere (IS) coordination at the center of a ditrigonal cavity of one surface and above  
11  
12 a Si tetrahedron on the other (Figure 3b), as well as being surrounded by 4-5  $\text{CO}_2$  molecules.  
13  
14 The  $\text{Cs}^+ - \text{O}_{\text{CO}_2}$  RCNs are essentially identical to those of Cs-hectorite exposed to dry  $\text{scCO}_2$   
15  
16 under same thermodynamic conditions, as expected due to the low  $\text{H}_2\text{O}$  content here.<sup>42</sup>  
17  
18 Importantly, the  $\text{Cs}^+ - \text{O}_{\text{CO}_2}$  RCN here is very similar to that of  $\text{Cs}^+ - \text{O}_{\text{H}_2\text{O}}$  in Cs-hectorite in  
19  
20 equilibrium with pure  $\text{H}_2\text{O}$ .<sup>49</sup> This result is in good agreement with our recent experimental  
21  
22 results, which suggest that replacement of  $\text{H}_2\text{O}$  by  $\text{CO}_2$  in the 1L structure of Cs-hectorite under  
23  
24 the conditions here requires only a small energy change.<sup>17</sup> The mean non-bonded  $\text{O}_{\text{CO}_2} - \text{O}_b$   
25  
26 and  $\text{O}_{\text{CO}_2} - \text{O}_{\text{CO}_2}$  interatomic distances in Cs-hectorite are centered at  $3.4 \text{ \AA}$  and  $3.2 \text{ \AA}$ ,  
27  
28 respectively, and the  $\text{O}_{\text{CO}_2} - \text{O}_b$  RCN is  $\sim 7.7$  (Figure 4a). The average local structure of the  $\text{CO}_2$   
29  
30 molecules is best characterized as having the  $\text{O}_{\text{CO}_2}$  atoms located above a silica tetrahedron of  
31  
32 one basal surface and above the center of a ditrigonal cavity of the other basal surface (Figure  
33  
34 3b). The  $\text{O}_{\text{CO}_2} - \text{O}_{\text{CO}_2}$  RCN is  $\sim 4.6$ , and their mutual arrangement is dominated by a slipped  
35  
36 parallel arrangement (parallel  $\text{CO}_2$  with slight offset) with only a small fraction of T-shaped  
37  
38 arrangements (Figure 3b).<sup>38</sup> The rapid reorientation of  $\text{CO}_2$  perpendicular to the O-C-O  
39  
40 molecular axis is well illustrated by the dispersed contours for  $\text{O}_{\text{CO}_2}$  in the 1L structure (Figure  
41  
42 S2).  
43  
44  
45  
46  
47  
48  
49  
50

51 In both the 1L and 2L structures of Ca-hectorite, the mean  $\text{Ca}^{2+} - \text{O}_{\text{H}_2\text{O}}$  distance is  $2.5 \text{ \AA}$ ,  
52  
53 similar to the value in bulk aqueous solutions (Figure 3c and 3e),<sup>75</sup> and the absence of nearest  
54  
55 neighbor cation- $\text{O}_{\text{CO}_2}$  coordination is the same as in Na-hectorite.<sup>40</sup> This later result is  
56  
57 consistent with the expectation that cations with large hydration energies and smaller  $\text{CO}_2$   
58  
59  
60



1  
2  
3 solvation energies prefer to be coordinated by H<sub>2</sub>O at all R.H.s.<sup>58,75</sup> In Ca-hectorite, the  
4  
5 intercalated CO<sub>2</sub> molecules occur in small clusters between the hydrated Ca<sup>2+</sup> ions (Figure 3d),  
6  
7 as also observed in previous MD simulations of Na-montmorillonite.<sup>38</sup> The adsorption  
8  
9 environment of the Ca<sup>2+</sup> ions is very similar to our previous results of hydrated Ca-hectorite  
10  
11 without CO<sub>2</sub>.<sup>51</sup>  
12  
13

14  
15 The local coordination environment of CO<sub>2</sub> in the 1L structure of Ca-hectorite is  
16  
17 significantly different than in Cs-hectorite, with one O<sub>CO2</sub> at the center of a ditrigonal cavity of  
18  
19 one surface and the other directly above an O<sub>b</sub> of the opposite basal surface (Figure 3d). The  
20  
21 adsorption environment of CO<sub>2</sub> molecules reported here is in good agreement with earlier  
22  
23 calculations for Na-hectorite under identical simulated conditions.<sup>40</sup> This structure is also in  
24  
25 agreement with the O<sub>CO2</sub>-O<sub>b</sub> RCN of ~7.0 (Figure 4b). The aggregation of CO<sub>2</sub> is mostly in  
26  
27 trimers (O<sub>CO2</sub>-O<sub>CO2</sub> RCN = 3.6) with a slipped parallel orientation. There is no evidence of T-  
28  
29 shaped arrangements, as is also observed in the 1L structure of Cs-hectorite. The total non-  
30  
31 bonded coordination of CO<sub>2</sub> in Ca-hectorite increases from 10.3 (7.1 O<sub>b</sub> : 3.2 O<sub>H2O</sub>) in the 1L  
32  
33 structure to 12.3 (4.0 O<sub>b</sub> : 8.3 O<sub>H2O</sub>) in the 2L structure, but the H<sub>2</sub>O coordination to O<sub>b</sub> atoms  
34  
35 in the 1L and 2L structures is nearly the same as in hydrated Ca-hectorite without CO<sub>2</sub>.<sup>51</sup> This  
36  
37 result demonstrates that the H<sub>2</sub>O to O<sub>b</sub> H-bonding is not significantly affected by the presence  
38  
39 of CO<sub>2</sub>. The mean O<sub>b</sub>-O<sub>CO2</sub> distances decrease from 3.6 Å to 3.3 Å as the basal spacing  
40  
41 increases from the 1L to 2L structures, suggesting a more compact arrangement in the 2L  
42  
43 structure. Despite having similar mean O<sub>CO2</sub>-O<sub>b</sub> and O<sub>CO2</sub>-O<sub>H2O</sub> interatomic distances, the RCN  
44  
45 values in Ca-hectorite are significantly smaller than in the simulations of Ca-montmorillonite  
46  
47 exposed to wet CO<sub>2</sub> fluid at 323 K and 90 bar due to the differences in layer charge and  
48  
49 location, as discussed above.<sup>34</sup> The average adsorption environments of the intercalated species  
50  
51 for cations, H<sub>2</sub>O and CO<sub>2</sub> in the 1L and 2L structures of Cs- and Ca-hectorites are further  
52  
53  
54  
55  
56  
57  
58  
59  
60

1  
2  
3 validated by the planar atomic density distributions discussed in the supporting information  
4  
5 (Figures S2-S6).  
6

7  
8 *Coordination times and dynamics of the interlayer species*  
9

10 The mean nearest neighbor coordination times among the different intercalated species  
11 (H<sub>2</sub>O, CO<sub>2</sub>, cations) and with surface O<sub>b</sub> atoms show that the charge compensating cations play  
12 a crucial role in dictating the overall interlayer dynamics (Table 2). For the 1L structures, the  
13 intermittent and continuous coordination times for the Ca<sup>2+</sup>-O<sub>b</sub> pair are an order of magnitude  
14 longer than for the Cs<sup>+</sup>-O<sub>b</sub> pair, in good agreement with previous MD simulations of hydrated  
15 hectorites under ambient conditions.<sup>51</sup> In the 1L structures of both Cs- and Ca-hectorite, the  
16 cation-O<sub>b</sub> coordination times are significantly longer than the O<sub>CO2</sub>-O<sub>b</sub> coordination times,  
17 reflecting the weaker interaction of the CO<sub>2</sub> with the clay surface compared to cations. In  
18 contrast, the O<sub>CO2</sub> spend similar times near O<sub>b</sub> and Cs<sup>+</sup> in the 1L structure, suggesting a constant  
19 exchange among these coordination environments. This exchange may be due to the  
20 reorientation of the CO<sub>2</sub> parallel to the surface, which is consistent with the delocalized PADD  
21 contours for CO<sub>2</sub> molecules (Figure S2). The O<sub>CO2</sub>-O<sub>H2O</sub> and O<sub>CO2</sub>-O<sub>b</sub> residence times are  
22 similar for both the 1L and 2L structure of Ca-hectorite, but these times are much shorter than  
23 those for Ca-O<sub>H2O</sub> and Ca-O<sub>b</sub>, indicating that the interactions of CO<sub>2</sub> with the surface and H<sub>2</sub>O  
24 are weaker than those of Ca<sup>2+</sup>. The longer coordination times of Ca<sup>2+</sup> with H<sub>2</sub>O than with O<sub>b</sub> is  
25 consistent with its large hydration energy.<sup>58</sup> For Ca-hectorite, all the coordination times for the  
26 2L structure are shorter than for the 1L structure, reflecting the higher probability for H<sub>2</sub>O  
27 molecules to exchange between the 1<sup>st</sup> and 2<sup>nd</sup> coordination spheres of Ca<sup>2+</sup> with CO<sub>2</sub> librating  
28 and hopping between surface sites. There are no residence time values for Ca-O<sub>CO2</sub> for the 1L  
29 and 2L structures of Ca-hectorite and O<sub>H2O</sub> coordination around Cs<sup>+</sup> and O<sub>CO2</sub> in 1L structure  
30 of Cs-hectorite, because such coordination does not occur, even for short periods of time  
31  
32  
33  
34  
35  
36  
37  
38  
39  
40  
41  
42  
43  
44  
45  
46  
47  
48  
49  
50  
51  
52  
53  
54  
55  
56  
57  
58  
59  
60

(Figures 3c-3f). Similarly, because  $\text{Ca}^{2+}$  is present in outer sphere coordination in the 2L structure, there are no  $\text{Ca-O}_b$  values for it.

## Conclusions

Our GCMD simulation studies indicate that the intercalation behavior of  $\text{CO}_2$  and  $\text{H}_2\text{O}$  in the interlayers of hectorite when in contact with a binary  $\text{H}_2\text{O}$ -saturated  $\text{scCO}_2$  fluid at 323 K and 90 bars strongly depends on the hydration and solvation properties of the exchangeable, charge compensating cations. The adsorption profiles provide direct evidence for  $\text{CO}_2$  intercalation in Cs-hectorite even under anhydrous conditions, as observed in recent experimental studies.<sup>17</sup> In contrast,  $\text{CO}_2$  intercalation in Ca-hectorite occurs only when there is at least a sub-monolayer of  $\text{H}_2\text{O}$  present in the interlayers, as is also the case for Na-smectites.<sup>17,25</sup> The maximum interlayer mole fraction for  $\text{CO}_2$  occurs near the 1L structure for both Cs- (12.5 Å) and Ca-hectorites (12.8 Å) and decreases with increasing basal spacing. The negligible  $\text{H}_2\text{O}$  content (~1.5%) present at the maximum  $\text{CO}_2$  content in Cs-hectorite clearly indicates that  $\text{Cs}^+$  has similar affinities for both  $\text{H}_2\text{O}$  and  $\text{CO}_2$ , in good agreement with experiments.<sup>17,58</sup> The calculated immersion energies show that at the simulated conditions the 1L (12.5 Å) and 2L (16.2 Å) structures represent the stable equilibrium states for Cs- and Ca-hectorite, respectively.

The structural and dynamical behavior of the  $\text{CO}_2$  molecules in the 1L and 2L structures are in full agreement with previous interpretations of  $^{13}\text{C}$  NMR SSB patterns.<sup>17</sup> The simulations show that  $\text{CO}_2$  molecules in the 1L structures are located at the interlayer midplane, have a mean O-C-O axis orientation parallel to the basal surface (though they wobble around this mean value), and undergo librational motion about an axis perpendicular to their O-C-O axis. The observed  $^{13}\text{C}$  MAS NMR CSA patterns demonstrate rapid reorientation about an axis perpendicular to their O-C-O axis and because they probe the time-averaged structure are consistent with wobbling around this axis.<sup>17</sup> In contrast, simulations show that the intercalated

1  
2  
3 CO<sub>2</sub> molecules in the 2L structure of Ca-hectorite are adsorbed closer to one of the basal  
4 surfaces and experience less restricted dynamics than in the 1L structure. The computations  
5 show that direct, nearest neighbor coordination of CO<sub>2</sub> with Cs<sup>+</sup> in the 1L structure, but no  
6 nearest neighbor CO<sub>2</sub>-Ca<sup>2+</sup> coordination in either the 1L or 2L structures of Ca-hectorite.  
7 Again, these results are in full agreement with *in situ* experimental NMR observations.<sup>17</sup> In the  
8 1L structure of Cs-hectorite Cs<sup>+</sup> ions are adsorbed in a 9-fold IS coordination with respect to  
9 the basal surfaces and are also coordinated to 4-5 CO<sub>2</sub>. In contrast, in the 1L structure of Ca-  
10 hectorite CO<sub>2</sub> molecules occur exclusively in small clusters between hydrated Ca<sup>2+</sup> ions, where  
11 they assume a predominantly slipped parallel orientation with respect to each other. In the 1L  
12 structure of Cs-hectorite, the CO<sub>2</sub> molecules have one O<sub>CO2</sub> above a Si tetrahedron of one  
13 surface and the other above the center of a ditrigonal cavity of the opposite surface. This  
14 arrangement is slightly altered in both the 1L and 2L structures of Ca-hectorite, in which one  
15 O<sub>CO2</sub> is above the center of a ditrigonal cavity but the other is above an O<sub>b</sub> on the opposite  
16 surface and not on top of a Si tetrahedron.

17  
18  
19 Overall, the computed intercalation structure, dynamics and compositions are in good  
20 agreement with the recent *in situ* XRD, IR and NMR experimental data of Bowers et al.<sup>17</sup>,  
21 highlighting the complementarity of spectroscopy and molecular modeling. The agreement  
22 between the experimental interpretations and those observed in the GCMD simulations  
23 suggests that GCMD methods can be broadly applicable in future studies of binary and more  
24 complex fluids in complex nanoconfined environments.

## 25 Acknowledgements

26  
27 All the calculations in this work were performed using computational resources at the  
28 National Energy Research Scientific Computing Center, which is supported by the Office of  
29 Science of the U.S. Department of Energy under ECARP No. m1649. The authors acknowledge  
30 iCER computational facility at Michigan State University for additional computational  
31  
32  
33  
34  
35  
36  
37  
38  
39  
40  
41  
42  
43  
44  
45  
46  
47  
48  
49  
50  
51  
52  
53  
54  
55  
56  
57  
58  
59  
60

1  
2  
3 resources. The work in this manuscript was supported by the United States Department of  
4 Energy, Office of Science, Office of Basic Energy Science, Chemical science, Biosciences,  
5 and Geosciences division through the sister grants DE-FG02-10ER16128 (Bowers, P.I.) and  
6 DE-FG02-08ER15929 (Kirkpatrick, P.I.). A.G.K. acknowledges financial support of the  
7 industrial chair “Storage and Disposal of Radioactive Waste” at the IMT-Atlantique, funded  
8 by ANDRA, Areva, and EDF, and of the European Union’s Horizon 2020 research and  
9 innovation program under grant agreements No. 640979 and 764810.  
10  
11  
12  
13  
14  
15  
16  
17  
18  
19

## 20 **Notes**

21  
22  
23 The authors declare no competing financial interest.  
24  
25

## 26 **Supporting Information**

27  
28 A brief discussion of residence time definitions, orientations of H<sub>2</sub>O dipole with respect  
29 to surface normal of Ca-hectorites for 1L and 2L structures. Details of the planar atomic density  
30 distributions of interlayer species for the 1L and 2L structures of Cs- and Ca-hectorites.  
31  
32  
33  
34  
35  
36  
37  
38  
39  
40  
41  
42  
43  
44  
45  
46  
47  
48  
49  
50  
51  
52  
53  
54  
55  
56  
57  
58  
59  
60

## References

1. Gauss, I. Role and Impact of CO<sub>2</sub>-Rock Interactions during CO<sub>2</sub> Storage in Sedimentary Rocks. *Int. J. Green. Gas Cont.* **2010**, *4*, 73-89.
2. Lackner, K. S. A Guide to CO<sub>2</sub> Sequestration. *Science* **2003**, *300*, 1677-1678.
3. Benson, S. M.; Cole, D. R. CO<sub>2</sub> Sequestration in Deep Sedimentary Formations. *Elements* **2008**, *4*, 325-331.
4. Rutqvist, J. The Geomechanics of CO<sub>2</sub> Storage in Deep Sedimentary Formations. *Geotech. Geol. Eng.* **2012**, *30*, 525-551.
5. Bickle, M. J. Geological Carbon Storage. *Nature Geosci.* **2009**, *2*, 815-818.
6. Plasynski, S. I.; Litynski, J.T.; McIlvried, H. G.; Vikara, D. M.; Srivastava, R. D. The Critical Role of Monitoring, Verification, and Accounting for Geological Carbon Dioxide Storage Projects. *Environ. Geosci.* **2011**, *18*, 19-34.
7. Bachu, S.; Bonijoly, D.; Bradshaw, J.; Burruss, R.; Holloway, S.; Christensen, N. P.; Mathiassen, O. M. CO<sub>2</sub> Storage Capacity Estimation: Methodology and Gaps. *Int. J. Green. Gas Cont.* **2007**, *1*, 430-443.
8. Bourg, I. C.; Beckingham, L. E.; DePaolo, D. J. Then Nanoscale Basis of CO<sub>2</sub> Trapping for Geologic Storage. *Environ. Sci. Technol.* **2015**, *49*, 10265-10284.
9. Edlmann, K.; Haszeldine, S.; McDermott, C. I. Experimental Investigation into Sealing Capability of Naturally Fractured Shale Caprocks to Supercritical Carbon Dioxide Flow. *Environ. Earth Sci.* **2013**, *70*, 3393-3409.
10. Cole, D. R.; Chialvo, A. A.; Rother, G.; Vlcek, L.; Cummings, P. T. Supercritical Fluid Behavior at Nanoscale Interfaces: Implications for CO<sub>2</sub> Sequestration in Geological Formations. *Philoso. Mag.* **2010**, *90*, 2339-2363.
11. Berrezueta, E.; Menendez, G-, L.; Breitner, D.; Luquot, L. Pore System Changes During Experimental CO<sub>2</sub> Injection into Detritic Rocks. Studies of Potential Storage Rocks from Some Sedimentary Basins of Spain. *Int. J. Green. Gas Cont.* **2013**, *4*, 73-89
12. Ross, D. J. K.; Bustin, R. M. The Importance of Shale Composition and Pore Structure upon Gas Storage Potential of Shale Gas Reservoirs. *Mari. Petro. Geo.* **2009**, *26*, 916-927.
13. Heller, R.; Zoback, M. Adsorption of Methane and Carbon Dioxide on Gas Shale and Pure Mineral Samples. *J. Unconv. Oil Gas Res.* **2014**, *8*, 14-24.
14. Middleton, R. S.; Carey J. W.; Currier, R. P.; Hyman, J. D.; Kang, Q.; Karra, S.; Martinez, J. J.-; Porter, M. L.; Viswanathan, H. S. Shale Gas and Non-Aqueous Fracturing Fluid: Opportunities and Challenges for Supercritical CO<sub>2</sub>. *Appl. Ener.* **2015**, *147*, 500-509.
15. Busch, A.; Bertier, P.; Gensterblum, Y.; Rother, G.; Spiers, C. J.; Zhang, M.; Wentinck, H. M. On Sorption and Swelling of CO<sub>2</sub> in Clays. *Geomech. Geophys. Geo-energ. Geo-resour.* **2016**, *2*, 111-130.
16. Hamm, L. M.; Bourg, I. C.; Wallace, A. F.; Rotenberg, B. Molecular Simulation of CO<sub>2</sub>- and CO<sub>3</sub>-Brine-Mineral Systems. *Reviews in Mineralogy and Geochemistry* **2013**, *77*, 189-228.
17. Bowers, G. M.; Schaef, H. T.; Loring, J. S.; Hoyt, D. W.; Burton, S. D.; Walter, E. D.; Kirkpatrick, R. J. Role of Cations in CO<sub>2</sub> Adsorption, Dynamics and Hydration in Smectite Clays under In Situ Supercritical CO<sub>2</sub> Conditions. *J. Phys. Chem. C* **2017**, *121*, 577-592.

18. Giesting, P.; Guggenheim, S.; van Groos, A. F. K.; Busch, A. Interaction of Carbon Dioxide with Na-Exchanged Montmorillonite at Pressures to 640 bar: Implications for CO<sub>2</sub> Sequestration. *Int. J. Green. Gas Cont.* **2012**, *8*, 73-81.
19. Giesting, P.; Guggenheim, S.; van Groos, A. F. K.; Busch, A. X-ray Diffraction Study of K- and Ca-Exchanged Montmorillonites in CO<sub>2</sub> Atmospheres. *Environ. Sci. Technol.* **2012**, *46*, 5623-5630.
20. Bowers, G. M.; Hoyt, D. W.; Burton, S. D.; Ferguson, B. O.; Varga, R.; Kirkpatrick, R. J. In Situ <sup>13</sup>C and <sup>23</sup>Na Magic Angle Spinning NMR Investigation of Supercritical CO<sub>2</sub> Incorporation in Smectite-Natural Organic Matter Composites. *J. Phys. Chem. C* **2014**, *118*, 3564-3573.
21. Wang, Z.; Felmy, A. R.; Thompson, C. J.; Loring, J. S.; Joly, A. G.; Rosso, K. M.; Schaef, H. T.; Dixon, D. A. Near-Infrared Spectroscopic Investigation of Water in Supercritical CO<sub>2</sub> and the effect of CaCl<sub>2</sub>. *Fluid Phase Equil.* **2013**, *338*, 155-163.
22. Lee, M.-S.; McGrail, B. P.; Glezakou, V.-A. Microstructural Response of Variably Hydrated Ca-rich Montmorillonite to Supercritical CO<sub>2</sub>. *Environ. Sci. Technol.* **2014**, *48*, 8612-8619.
23. Ilton, E. S.; Schaef, H. T.; Qafoku, O.; Rosso, K. M.; Felmy, A. R. In Situ X-ray Diffraction Study of Na<sup>+</sup> Saturated Montmorillonite Exposed to Variably Wet Supercritical CO<sub>2</sub>. *Environ. Sci. Technol.* **2012**, *46*, 4241-4248.
24. Guggenheim, S.; van Groos, A. F. K. An Integrated Experimental System for Solid-Gas-Liquid Environmental Cells. *Clays Clay Miner.* **2014**, *62*, 470-476.
25. Rother, G.; Ilton, E. S.; Wallacher, D.; Hauss, T.; Schaef, H. T.; Qafoku, O.; Rosso, K. M.; Felmy, A. R.; Krukowski, E. G.; Stack, A. G.; et al. CO<sub>2</sub> Sorption to Subsingle Hydration Layer Montmorillonite Clay Studies by Excess Sorption and Neutron Diffraction Measurements. *Environ. Sci. Technol.* **2013**, *47*, 205-211.
26. Schaef, H. T.; Ilton, E. S.; Qafoku, O.; Martin, P. F.; Felmy, A. R.; Rosso, K. M. In Situ XRD study of Ca<sup>2+</sup> Saturated Montmorillonite (STx-1) Exposed to Anhydrous and Wet Supercritical Carbon Dioxide. *Int. J. Green. Gas Cont.* **2012**, *6*, 220-229.
27. Romanov, V. N. Evidence of Irreversible CO<sub>2</sub> Intercalation in Montmorillonite. *Int. J. Green. Gas Cont.* **2013**, *14*, 220-226.
28. Schaef, H. T.; Loring, J. S.; Glezakou, V. A.; Miller, Q. R. S.; Chen, J.; Owen, A. T.; Lee, M.-S.; Ilton, E. S.; Felmy, A. R.; McGrail, B. P. et al. Competitive Sorption of CO<sub>2</sub> and H<sub>2</sub>O in 2:1 Layer Phyllosilicates. *Geochim. Cosmochim. Acta* **2015**, *161*, 248-257.
29. Loring, J. S.; Schaef, H. T.; Turcu, R. V. F.; Thompson, C. J.; Miller, Q. R.; Martin, P. F.; Hu, J.; Hoyt, D. W.; Qafoku, O.; Ilton, E. S.; et al. In Situ Molecular Spectroscopic Evidence for CO<sub>2</sub> Intercalation into Montmorillonite in Supercritical Carbon Dioxide. *Langmuir* **2012**, *28*, 7125-7128.
30. Loring, J.S.; Ilton, E.S.; Chen, J.; Thompson, C.J.; Martin, P.F.; Benezeth, P.; Rosso, K.M.; Felmy, A.R.; Schaef, H.T. In Situ Study of CO<sub>2</sub> and H<sub>2</sub>O Partitioning Between Na-Montmorillonite and Variably Wet Supercritical Carbon Dioxide. *Langmuir* **2014**, *30*, 6120-6128.
31. Loring, J. S.; Schaef, H. T.; Thompson, C. J.; Turcu, R. V. F.; Miller, Q. R.; Chen, J.; Hu, J.; Hoyt, D. W.; Martin, P. F.; Ilton, E. S.; et al. Clay Hydration/Dehydration in Dry to

- 1  
2  
3 Water-Saturated Supercritical CO<sub>2</sub>: Implications for Caprock Integrity. *Energy Procedia*  
4 **2013**, *37*, 5443-5448.  
5
- 6 32. Krukowski, E.G.; Goodman, A.; Rother, G.; Ilton, E.S.; Guthrie, G.; Bodnar, R.J. FT-IR  
7 Study of CO<sub>2</sub> Interaction with Na<sup>+</sup> Exchanged Montmorillonite. *Appl. Clay Sci.* **2015**, *114*,  
8 61-68.  
9
- 10 33. Botan, A.; Rotenberg, R.; Marry, V.; Turq, P.; Noetinger, B. Carbon Dioxide in  
11 Montmorillonite Clay Hydrates: Thermodynamics, Structure and Transport from  
12 Molecular Simulation. *J. Phys. Chem. C* **2010**, *114*, 14962-14969.  
13
- 14 34. Kadoura, A.; Nair, A. K. N.; Sun, S. Molecular Simulation Study of Montmorillonite in  
15 Contact with Variably Wet Supercritical Carbon Dioxide. *J. Phys. Chem. C* **2017**, *121*,  
16 6199-6208.  
17
- 18 35. Myshakin, E. M.; Saidi, W. A.; Romanov, V. N.; Cygan, R. T.; Jordan, K. D. Molecular  
19 Dynamics Simulations of Carbon Dioxide Intercalation in Hydrated Na-Montmorillonite.  
20 *J. Phys. Chem. C* **2013**, *117*, 11028-11039.  
21
- 22 36. Makaremi, M.; Jordan, K. D.; Guthrie, G. D.; Myshakin, E. M. Multiphase Monte Carlo  
23 and Molecular Dynamics Simulations of Water and CO<sub>2</sub> Intercalation in Montmorillonite  
24 and Beidellite. *J. Phys. Chem. C* **2015**, *119*, 15112-15124.  
25
- 26 37. Rao, A.; Leng, Y. Effect of Layer Charge on CO<sub>2</sub> and H<sub>2</sub>O Intercalations in Swelling Clays.  
27 *Langmuir* **2016**, *32*, 11366-11374.  
28
- 29 38. Sena, M. M.; Morrow, C. P.; Kirkpatrick, R. J.; Krishnan, M. Structure, Energetics, and  
30 Dynamics of Supercritical Carbon Dioxide at Smectite Mineral-Water Interfaces:  
31 Molecular Dynamics Modeling and Adaptive Force Investigation of CO<sub>2</sub>/H<sub>2</sub>O Mixtures  
32 Confined in Na-Montmorillonite. *Chem. Mater.* **2015**, *27*, 6946-6959.  
33
- 34 39. Yazaydin, A. O.; Bowers, G. M.; Kirkpatrick, R. J. Molecular Dynamics Modeling of  
35 Carbon Dioxide, Water and Natural Organic Matter in Na-Hectorite. *Phys. Chem. Chem.*  
36 *Phys.* **2015**, *17*, 23356-23367.  
37
- 38 40. Loganathan, N.; Yazaydin, A. O.; Bowers, G. M.; Kalinichev, A. G.; Kirkpatrick, R. J.  
39 Molecular Dynamics Study of CO<sub>2</sub> and H<sub>2</sub>O Intercalation in Smectite Clays: Effect of  
40 Temperature and Pressure on Interlayer Structure and Dynamics in Hectorite *J. Phys.*  
41 *Chem. C* **2017**, *121*, 24527-24540.  
42
- 43 41. Schaefer, H. T.; Loganathan, N.; Bowers, G. M.; Kirkpatrick, R.; Yazaydin, A. O.; Burton,  
44 S. D.; Hoyt, D. W.; Ilton, E. S.; Thanthiriwatte, K. S.; Dixon, D. A. et al. Tipping Point for  
45 Expansion of Layered Aluminosilicates in Weakly Polar Solvents: Supercritical CO<sub>2</sub>. *ACS*  
46 *Appl. Mater. Interf.* **2017**, *9*, 36783-36791.  
47
- 48 42. Loganathan, N.; Bowers, G. M.; Yazaydin, A. O.; Schaefer, H. T.; Loring, J.; Kalinichev, A.  
49 G.; Kirkpatrick, R. J. Clay Swelling in Dry Supercritical Carbon Dioxide: Effects of  
50 Interlayer Cations on the Structure, Dynamics and Energetics of CO<sub>2</sub> Intercalation Probed  
51 by XRD, NMR and GCMD Simulations. *J. Phys. Chem. C* **2018**, *122*, 4391-4402.  
52
- 53 43. Bowers, G. M.; Singer, J. W.; Bish, D. L.; Kirkpatrick, R. J. Alkali Metal and H<sub>2</sub>O  
54 Dynamics at the Clay/Water Interface. *J. Phys. Chem. C* **2011**, *115*, 23395-23407.  
55
- 56 44. Marry, V.; Dubois, E.; Malikova, N.; Durand-Vidal, S.; Longeville, S.; Breu, J. Water  
57 Dynamics in Hectorite Clays: Influence of Temperature Studied by Coupling Neutron Spin  
58 Echo and Molecular Dynamics. *Environ. Sci. Technol.* **2011**, *45*, 2850-2855.  
59  
60



- 1
  - 2
  - 3
  - 4
  - 5
  - 6
  - 7
  - 8
  - 9
  - 10
  - 11
  - 12
  - 13
  - 14
  - 15
  - 16
  - 17
  - 18
  - 19
  - 20
  - 21
  - 22
  - 23
  - 24
  - 25
  - 26
  - 27
  - 28
  - 29
  - 30
  - 31
  - 32
  - 33
  - 34
  - 35
  - 36
  - 37
  - 38
  - 39
  - 40
  - 41
  - 42
  - 43
  - 44
  - 45
  - 46
  - 47
  - 48
  - 49
  - 50
  - 51
  - 52
  - 53
  - 54
  - 55
  - 56
  - 57
  - 58
  - 59
  - 60
45. Bowers, G. M.; Singer, J. W.; Bish, D. L.; Kirkpatrick, R. J. Structure and Dynamical Relationships of  $\text{Ca}^{2+}$  and  $\text{H}_2\text{O}$  in Smectite/ $^2\text{H}_2\text{O}$  Systems. *Amer. Mineral.* 2014, 99, 318-331.
46. Weiss, C. A.; Kirkpatrick, R. J.; Altaner, S. P. Variations in Interlayer Cation Sites of Clay Minerals as Studied by  $^{133}\text{Cs}$  MAS Nuclear Magnetic Resonance Spectroscopy. *Amer. Mineral.* **1990**, 75, 970-982.
47. Weiss, C. A.; Kirkpatrick, R. J.; Altaner, S. P. The Structural Environments of Cations Adsorbed onto Clays –  $^{133}\text{Cs}$  Variable-Temperature MAS NMR Spectroscopic Study of Hectorite. *Geochim. Cosmochim. Acta* **1990**, 54, 1655-1669.
48. Reddy, U. V.; Bowers, G. M.; Loganathan, N.; Bowden, M.; Yazaydin, A. O.; Kirkpatrick, R. J. Water Structure and Dynamics in Smectites:  $^2\text{H}$  NMR Spectroscopy of Mg, Ca, Sr, Cs and Pb-Hectorite. *J. Phys. Chem. C* **2016**, 120, 8863-8876.
49. Loganathan, N.; Yazaydin, A. O.; Bowers, G. M.; Kalinichev, A. G.; Kirkpatrick, R. J. Structure, Energetics and Dynamics of  $\text{Cs}^+$  and  $\text{H}_2\text{O}$  in Hectorite: Molecular Dynamics Simulations with Unconstrained Substrate Surface. *J. Phys. Chem. C* **2016**, 120, 10298-10310.
50. Porion, P.; Faugere, A. M.; Delville, A. Multiscale Water Dynamics within Dense Clay Sediments Probed by  $^2\text{H}$  Multiquantum NMR Relaxometry and Two-Time Stimulated Echo NMR Spectroscopy. *J. Phys. Chem. C* **2013**, 117, 26119-26134.
51. Loganathan, N.; Yazaydin, A. O.; Bowers, G. M.; Kalinichev, A. G.; Kirkpatrick, R. J. Cation and Water Structure, Dynamics and Energetics in Smectite Clays: A Molecular Dynamics Study of Ca-Hectorite. *J. Phys. Chem. C* **2016**, 120, 12429-12439.
52. Morrow, C. P.; Yazaydin, A. O.; Krishnan, M.; Bowers, G. M.; Kalinichev, A. G.; Kirkpatrick, R. J. Structure, Energetics and Dynamics of Smectite Clay Interlayer Hydration: Molecular Dynamics and Metadynamics Investigation of Na-Hectorite. *J. Phys. Chem. C* **2013**, 117, 5172-5187.
53. Greathouse, J. A.; Hart, D. B.; Bowers, G. M.; Kirkpatrick, R. J.; Cygan, R. T. Molecular Simulation of Structure and Diffusion at Smectite-Water Interfaces: Using Expanded Clay Interlayers as Model Nanopores. *J. Phys. Chem. C* **2015**, 119, 17126-17136.
54. Ngouana-Wakou, B.F.; Kalinichev, A.G. Structural Arrangements of Isomorphic Substitutions in Smectites: Molecular Simulation of the Swelling Properties, Interlayer Structure and Dynamics of Hydrated Cs-Montmorillonite Revisited with New Clay Models. *J. Phys. Chem. C* **2014**, 118, 12758-12773.
55. Loganathan, N.; Kalinichev, A. G. On the Hydrogen Bonding Structure at the Aqueous Interface of Ammonium-Substituted-Mica: A Molecular Dynamics Simulation. *Z. Naturforsch., A: Phys. Sci.* **2013**, 68a, 91-100.
56. Sato, T.; Watanabe, T.; Otuka, R. Effects of Layer Charge, Charge Location, and Energy Change on Expansion Properties of Dioctahedral Smectites. *Clays Clay Miner.* **1992**, 29, 873-882.
57. Loganathan, N.; Kalinichev, A. G. Quantifying the Mechanisms of Site-Specific Ion Exchange at an Inhomogeneously Charged Surface. Case of  $\text{Cs}^+/\text{K}^+$  on Hydrated Muscovite Mica. *J. Phys. Chem. C* **2017**, 121, 7829-7836.
58. Criscenti, L. J.; Cygan, R. T., Molecular Simulations of Carbon Dioxide and Water: Cation Solvation. *Environ. Sci. Technol.* **2013**, 47, 87-94.

- 1  
2  
3 59. Breu, J.; Seidl, W.; Stoll, A., Disorder in Smectites in Dependence of the Interlayer Cation. *Z. Anorg. Allg. Chem.* **2003**, *629*, 503-515.
- 4  
5  
6 60. Tenorio, R. P.; Alme, L. R.; Engelsberg, M.; Fossum, J. O.; Hallwass, F. Geometry and  
7 Dynamics of Intercalated Water in Na-Fluorohectorite Clay Hydrates. *J. Phys. Chem. C*  
8 **2008**, *112*, 575-580.
- 9  
10 61. Lowenstein, W. The Distribution of Aluminium in the Tetrahedra of Silicates and  
11 Aluminates. *Am. Mineral.* **1954**, *39*, 92-96.
- 12  
13 62. Boinepalli, S.; Attard, P. Grand Canonical Molecular Dynamics. *J. Chem. Phys.* **2003**, *119*,  
14 12769-12775.
- 15  
16 63. Dubbeldam, D.; Calero, S.; Ellis, D. E.; Snurr, R. Q. RASPA: Molecular Simulation  
17 Software for Adsorption and Diffusion in Flexible Nanoporous Materials. *Mol. Simul.*  
18 **2016**, *42*, 81-101.
- 19  
20 64. Cygan, R. T.; Liang, J.-J.; Kalinichev, A. G. Molecular Models of Hydroxide,  
21 Oxyhydroxide and Clay Phases and the Development of a General Force Field. *J. Phys.*  
22 *Chem. B* **2004**, *108*, 1255-1266.
- 23  
24 65. Berendsen, H. J. C.; Postma, J. P. M.; Gunsteren, W. F.; van Hermans, J. Interaction Models  
25 for Water in Relation to Protein Hydration. In *Intermolecular Forces*; The Jerusalem  
26 Symposia on Quantum Chemistry and Biochemistry; Pullman, B., Ed.; Springer:  
27 Netherlands, 1981; pp 331–342.
- 28  
29 66. Cygan, R. T.; Romanov, V. N.; Myshakin, E. M. Molecular Simulation of Carbon Dioxide  
30 Capture by Montmorillonite Using an Accurate and Flexible Force Field. *J. Phys. Chem. C*  
31 **2012**, *116*, 13079-13091.
- 32  
33 67. Allen, M. P.; Tildesley, D. J. *Computer Simulations of Liquids*; 2<sup>nd</sup> edition. Oxford  
34 University Press: Oxford, U.K., 2017.
- 35  
36 68. Spycher, N.; Pruess, K.; Ennis-King J. CO<sub>2</sub>-H<sub>2</sub>O Mixtures in the Geological Sequestration  
37 fom 12 to 100° and up to 600 bar. *Geochim. Cosmochim. Acta* **2003**, *67*, 3015-3031.
- 38  
39 69. Peng, D. Y.; Robinson, D. B. A New Two-Constant Equation of State. *Ind. Eng. Chem.*  
40 *Fundam.* **1976**, *15*, 59-64.
- 41  
42 70. Smith, D. E. Molecular Computer Simulations of the Swelling Properties and Interlayer  
43 Structure of Cesium Montmorillonite. *Langmuir* **1998**, *14*, 5959-5967.
- 44  
45 71. Young, D. A.; Smith, D. E. Simulations of Clay Mineral Swelling and Hydration:  
46 Dependence upon Interlayer Ion Size and Charge. *J. Phys. Chem. B* **2000**, *104*, 9163-9170.
- 47  
48 72. Shroll, R.; Smith, D. E. Molecular Dynamics Simulations in the Grand Canonical  
49 Ensemble: Application to Clay Mineral Swelling. *J. Chem. Phys.* **1999**, *111*, 9025-9033.
- 50  
51 73. Whitley, H. D.; Smith, D. E. Free Energy, Energy and Entropy of Swelling in Cs-, Na-, and  
52 Sr-Montmorillonite Clays. *J. Chem. Phys.* **2004**, *120*, 5387-5395.
- 53  
54 74. Dazas, B.; Lanson, B.; Breu, J.; Robert, J.-L.; Pelletier, M.; Ferrage, E. Smectite  
55 Fluorination and its Impact on Interlayer Water Content and Structure: A Way to Fine Tune  
56 the Hydrophilicity of Clay Surfaces. *Micro. Meso. Mat.* **2013**, *181*, 233-247.
- 57  
58 75. Ohtaki, H.; Radnai, T. Structure and Dynamics of Hydrated Ions. *Chem. Rev.* **1993**, *93*,  
59 1157-1204.
- 60

**Table 1.** CO<sub>2</sub> mole fraction at equilibrium interlayer distances for Cs- and Ca-hectorites at 323 K and 90 bar in comparison to experimental results.

	Interlayer distance	Interlayer mole fraction of CO <sub>2</sub>	
		(Simulations)	(Experiments) <sup>17</sup>
<b>Cs – hectorite</b>	Monolayer (12.5 Å)	0.98	0.34 - 0.82 (12.2 Å)
<b>Ca – hectorite</b>	Monolayer (12.7 Å)	0.34	0.13 - 0.54 (12.0 Å)
	Bilayer (16.2 Å)	0.02	0.02 - 0.42 (15.8 Å)
<b>Na – hectorite</b>	Monolayer (12.5 Å) <sup>40</sup>	0.18	0.05 - 0.14
	Bilayer (15.5 Å) <sup>40</sup>	0.03	

**Table 2.** Calculated intermittent and continuous residence times (*ns*) for the listed atomic pairs in the interlayers of Cs- and Ca-hectorite at 323 K and 90 bar.

basal spacing (Å)	Ion-O <sub>H2O</sub>	Ion-O <sub>b</sub>	Ion-O <sub>CO2</sub>	O <sub>H2O</sub> -O <sub>b</sub>	O <sub>b</sub> -O <sub>CO2</sub>	O <sub>H2O</sub> -CO <sub>2</sub>
<b><math>\tau_{int}</math> (res): <math>\tau_{cont}</math> (res)</b>						
<i>Ca-hectorite</i>						
1L (12.8Å)	21 : 3	12 : 1	- : -	2 : 0.4	0.5 : 0.05	0.5 : 0.1
2L (16.2Å)	1.9 : 0.5	- : -	- : -	0.4 : 0.1	0.1 : 0.03	0.1 : 0.02
<i>Cs-hectorite</i>						
1L (12.5Å)	- : -	0.9 : 0.05	0.4 : 0.02	- : -	0.5 : 0.03	- : -

## FIGURES

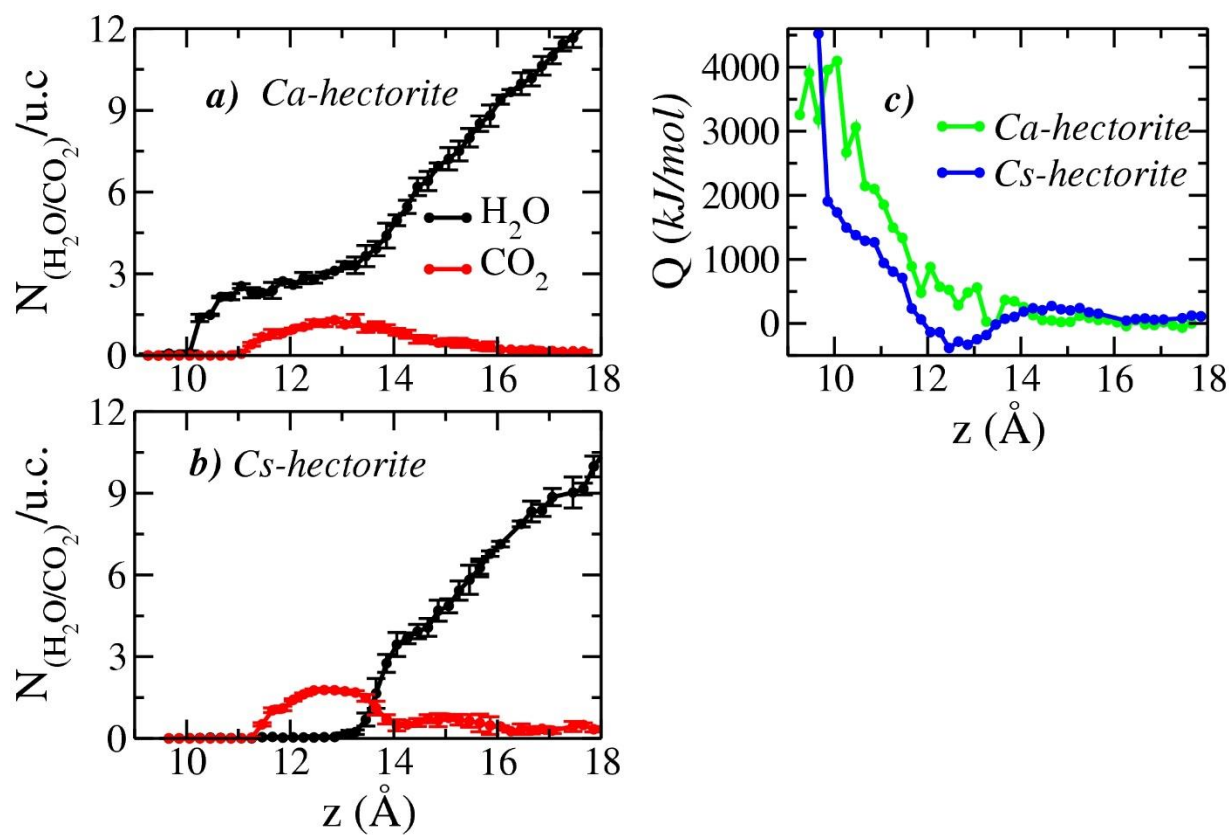


**Figure 1.** a) and b): Average number of intercalated  $\text{CO}_2$  and  $\text{H}_2\text{O}$  molecules per unit cell in Ca- and Cs-hectorite as functions of interlayer basal spacing at 323 K and 90 bar. c): The computed immersion energies for the same systems.

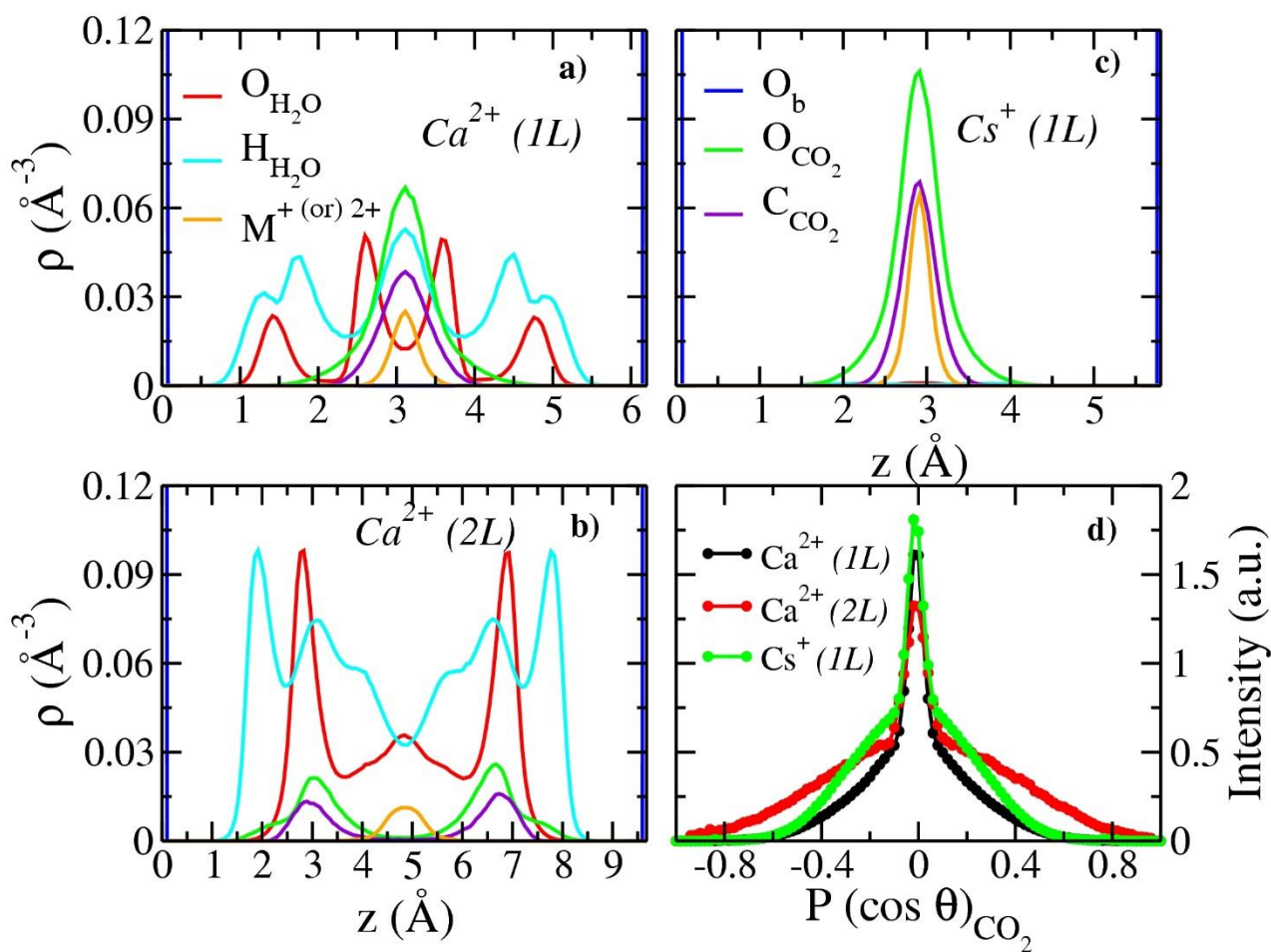


**Figure 2.** a), b), c): Computed atomic density profiles (ADPs) of  $\text{O}_b$  (dark blue vertical lines), the exchangeable cation (orange),  $\text{O}_{\text{H}_2\text{O}}$  (red),  $\text{H}_{\text{H}_2\text{O}}$  (cyan),  $\text{O}_{\text{CO}_2}$  (green) and  $\text{C}_{\text{CO}_2}$  (violet) in Cs- and Ca-hectorite as functions of distance from the basal clay surface at 323 K and 90 bar. a) and b) 1L and 2L structures of Ca-hectorite. The ADPs of  $\text{O}_{\text{CO}_2}$  and  $\text{C}_{\text{CO}_2}$  in 2b are enhanced 5 times than their original values to improve visibility. c) 1L structure of Cs-hectorite. d) Computed orientation distributions of intercalated  $\text{CO}_2$  molecules in the interlayers of Ca- and Cs-hectorite at 323 K and 90 bar.  $P(\cos \theta)_{\text{CO}_2}$  is the cosine of the angle between the O-O vector of the  $\text{CO}_2$  molecules and the normal to the hectorite basal surface. The intensity of the distribution for the 2L Ca-hectorite is enhanced 10X for better illustrations.

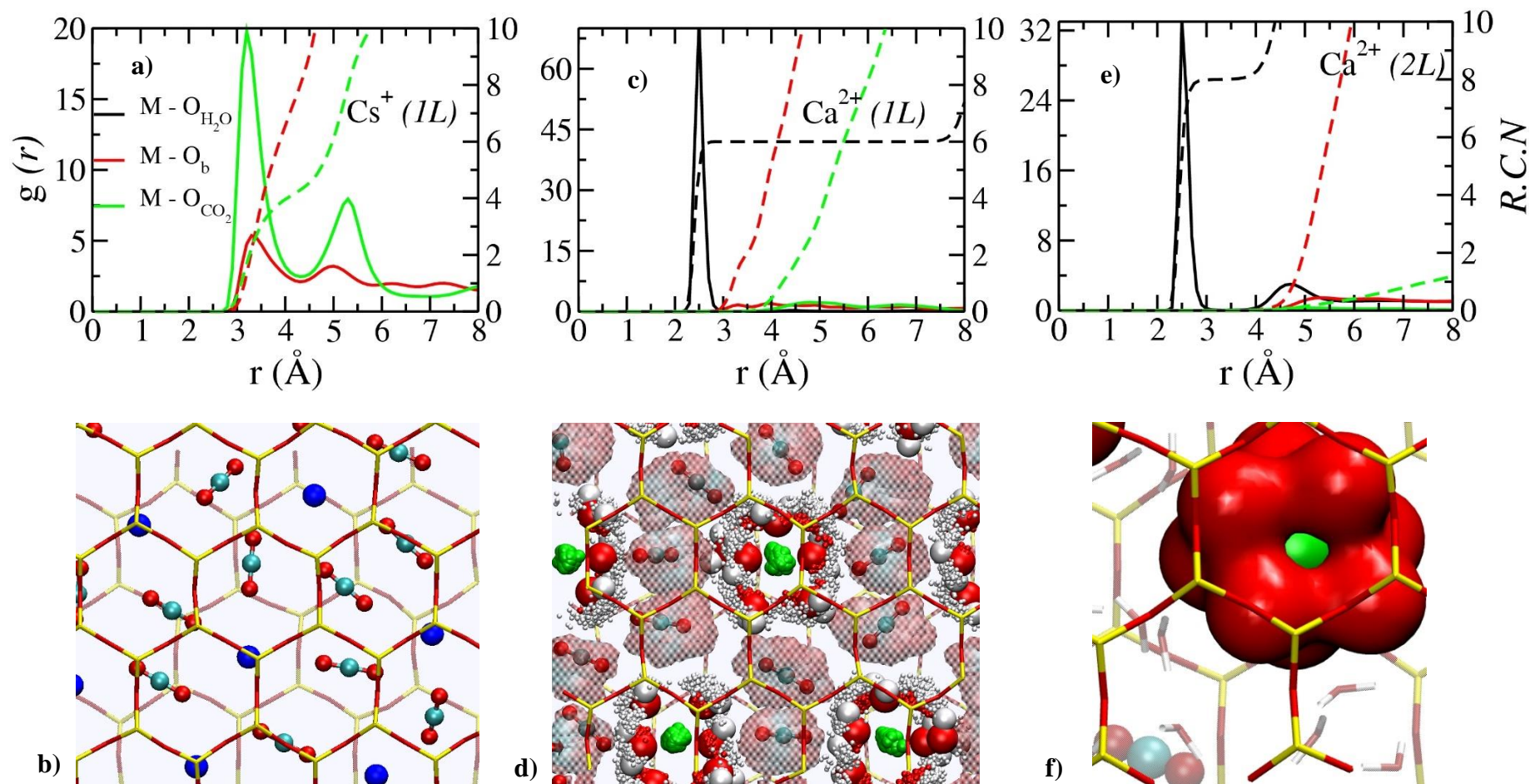


**Figure 3.** a), c), e): Radial distribution functions (RDFs, solid lines) and corresponding running coordination numbers (RCNs, dashed lines) for the indicated atomic pairs involving Cs<sup>+</sup> and Ca<sup>2+</sup> ions in the interlayers of hectorite at 323 K and 90 bar. a) 1L of Cs-hectorite. b) 1L of Ca-hectorite. c) 2L of Ca-hectorite. M – Cation. b) pictorial representation of intercalated CO<sub>2</sub> and Cs<sup>+</sup> in 1L structure of Cs-hectorite; d) pictorial

1  
2  
3 representation of average positions for CO<sub>2</sub>, H<sub>2</sub>O and Ca<sup>2+</sup> in 1L Ca-hectorite; f) pictorial representation of nearest neighbour H<sub>2</sub>O around Ca<sup>2+</sup>  
4  
5 ions in 2L Ca-hectorite. Color codes: blue – Cs<sup>+</sup>; green – Ca<sup>2+</sup>; red – O<sub>H2O</sub>/O<sub>CO2</sub>; cyan – C<sub>CO2</sub>; white – H<sub>H2O</sub>; Bright and shaded red and yellow  
6  
7 sticks corresponds to surface oxygen (O<sub>b</sub>) and silicon atoms.  
8  
9  
10  
11  
12  
13  
14  
15  
16  
17  
18  
19  
20  
21  
22  
23  
24  
25  
26  
27  
28  
29  
30  
31  
32  
33  
34  
35  
36  
37  
38  
39  
40  
41  
42  
43  
44  
45  
46

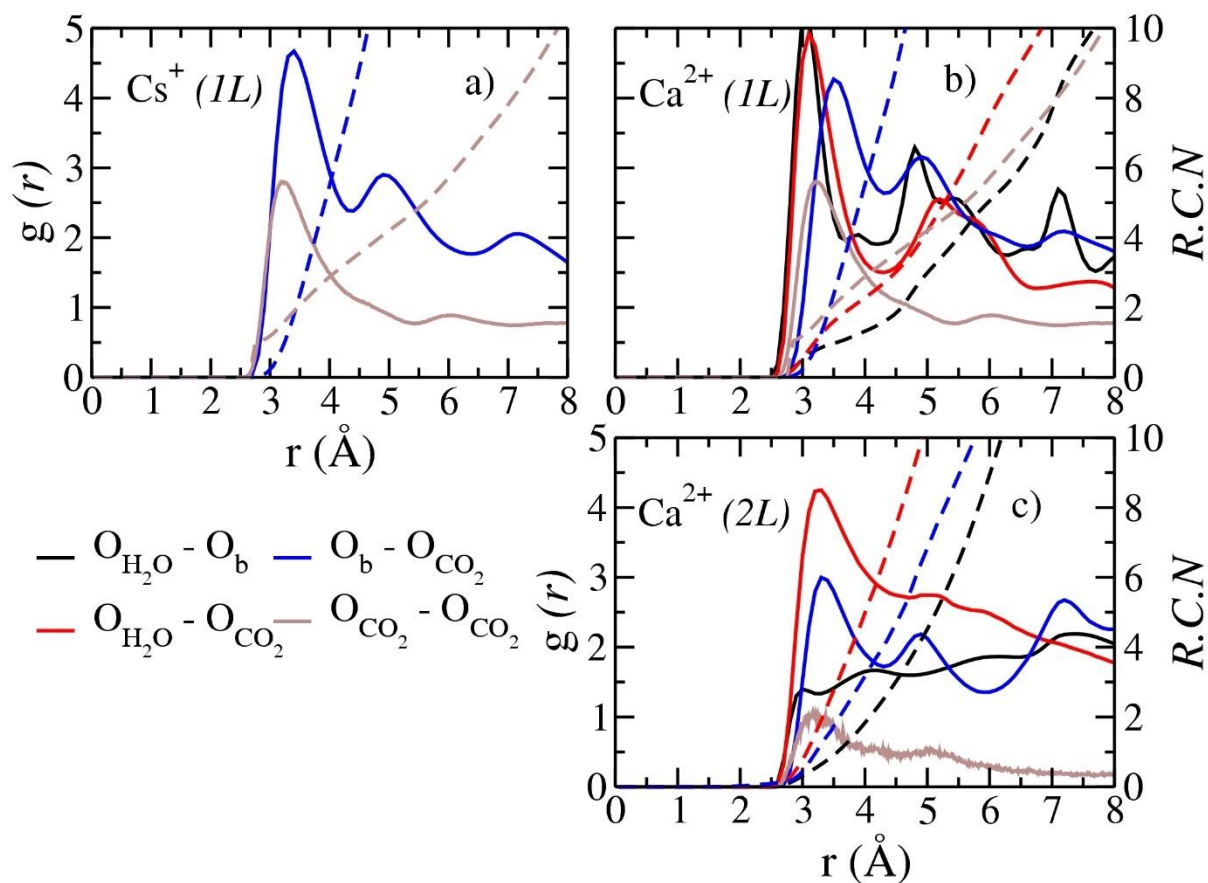


**Figure 4.** Radial distribution functions (RDFs, solid lines) and corresponding running coordination numbers (RCNs, dashed lines) for non-bonded O atomic pairs in Cs- and Ca-hectorites at 323 K and 90. a) 1L of Cs-hectorite. b) 1L of Ca-hectorite. c) 2L of Ca-hectorite.



**TOC Graphic**